



HAL
open science

Dependence of the evolution of carbon dynamics in the northern permafrost region on the trajectory of climate change

David Mcguire, David Lawrence, Charles Koven, Joy Clein, Eleanor Burke, Guangsheng Chen, Elchin Jafarov, Andrew Macdougall, Sergey Marchenko, Dmitry Nicolsky, et al.

► To cite this version:

David Mcguire, David Lawrence, Charles Koven, Joy Clein, Eleanor Burke, et al.. Dependence of the evolution of carbon dynamics in the northern permafrost region on the trajectory of climate change. Proceedings of the National Academy of Sciences of the United States of America, 2018, 115 (15), pp.3882 - 3887. 10.1073/pnas.1719903115 . hal-01806825

HAL Id: hal-01806825

<https://hal.science/hal-01806825>

Submitted on 16 May 2020

HAL is a multi-disciplinary open access archive for the deposit and dissemination of scientific research documents, whether they are published or not. The documents may come from teaching and research institutions in France or abroad, or from public or private research centers.

L'archive ouverte pluridisciplinaire **HAL**, est destinée au dépôt et à la diffusion de documents scientifiques de niveau recherche, publiés ou non, émanant des établissements d'enseignement et de recherche français ou étrangers, des laboratoires publics ou privés.



Dependence of the evolution of carbon dynamics in the northern permafrost region on the trajectory of climate change

A. David McGuire^{a,1}, David M. Lawrence^b, Charles Koven^c, Joy S. Clein^d, Eleanor Burke^e, Guangsheng Chen^{f,g}, Elchin Jafarov^h, Andrew H. MacDougallⁱ, Sergey Marchenko^j, Dmitry Nicolsky^j, Shushi Peng^{k,l}, Annette Rinke^{m,n}, Philippe Ciais^k, Isabelle Gouttevin^{l,o}, Daniel J. Hayes^{f,p}, Duoying Jiⁿ, Gerhard Krinner^l, John C. Moore^{n,q,r}, Vladimir Romanovsky^{j,s}, Christina Schädel^{t,u}, Kevin Schaefer^v, Edward A. G. Schuur^{t,u}, and Qianlai Zhuang^w

^aUS Geological Survey, Alaska Cooperative Fish and Wildlife Research Unit, University of Alaska Fairbanks, Fairbanks, AK 99775; ^bClimate and Global Dynamics Laboratory, National Center for Atmospheric Research, Boulder, CO 80305; ^cClimate and Ecosystem Sciences Division, Lawrence Berkeley National Laboratory, Berkeley, CA 94720; ^dInstitute of Arctic Biology, University of Alaska Fairbanks, Fairbanks, AK 99775; ^eMet Office Hadley Centre, EX1 3PB Exeter, United Kingdom; ^fEnvironmental Sciences Division, Oak Ridge National Laboratory, Oak Ridge, TN 37830; ^gInternational Center for Climate and Global Change Research, Auburn University, Auburn, AL 36849; ^hEarth and Environmental Sciences Division, Los Alamos National Laboratory, Los Alamos, NM 87545; ⁱDepartment of Earth Sciences, St. Francis Xavier University, Antigonish, NS, Canada B2G 2W5; ^jGeophysical Institute, University of Alaska Fairbanks, Fairbanks, AK 99775; ^kLaboratoire des Sciences du Climat et de l'Environnement, Commissariat à l'Energie Atomique–CNRS–Université de Versailles Saint-Quentin-en-Yvelines, UMR8212, 91191 Gif-sur-Yvette, France; ^lInstitut des Geosciences de l'Environnement, Université Grenoble Alpes, CNRS, F-38000 Grenoble, France; ^mAlfred Wegener Institute, Helmholtz Centre for Polar and Marine Research, 14473 Potsdam, Germany; ⁿCollege of Global Change and Earth System Science, Beijing Normal University, Beijing 100875, China; ^oIrstea, Hydrology–Hydraulics Research Unit, 69616 Villeurbanne Cedex, France; ^pSchool of Forest Resources, University of Maine, Orono, ME 04469; ^qArctic Centre, University of Lapland, 96101 Rovaniemi, Finland; ^rCenter for Excellence in Tibetan Plateau Earth Sciences, Chinese Academy of Sciences, Beijing 100101, China; ^sInternational Institute of Cryology and Cryosphy, Tyumen State University, 625003 Tyumen, Russia; ^tCenter for Ecosystem Science and Society, Northern Arizona University, Flagstaff, AZ 86011; ^uDepartment of Biological Sciences, Northern Arizona University, Flagstaff, AZ 86011; ^vNational Snow and Ice Data Center, University of Colorado, Boulder, CO 80303; and ^wDepartment of Earth, Atmospheric, and Planetary Sciences, Purdue University, West Lafayette, IN 47907

Edited by William H. Schlesinger, Earth and Ocean Sciences, Nicholas School of the Environment, Duke University, Durham, NC, and approved January 29, 2018 (received for review November 14, 2017)

We conducted a model-based assessment of changes in permafrost area and carbon storage for simulations driven by RCP4.5 and RCP8.5 projections between 2010 and 2299 for the northern permafrost region. All models simulating carbon represented soil with depth, a critical structural feature needed to represent the permafrost carbon–climate feedback, but that is not a universal feature of all climate models. Between 2010 and 2299, simulations indicated losses of permafrost between 3 and 5 million km² for the RCP4.5 climate and between 6 and 16 million km² for the RCP8.5 climate. For the RCP4.5 projection, cumulative change in soil carbon varied between 66-Pg C (10¹⁵-g carbon) loss to 70-Pg C gain. For the RCP8.5 projection, losses in soil carbon varied between 74 and 652 Pg C (mean loss, 341 Pg C). For the RCP4.5 projection, gains in vegetation carbon were largely responsible for the overall projected net gains in ecosystem carbon by 2299 (8- to 244-Pg C gains). In contrast, for the RCP8.5 projection, gains in vegetation carbon were not great enough to compensate for the losses of carbon projected by four of the five models; changes in ecosystem carbon ranged from a 641-Pg C loss to a 167-Pg C gain (mean, 208-Pg C loss). The models indicate that substantial net losses of ecosystem carbon would not occur until after 2100. This assessment suggests that effective mitigation efforts during the remainder of this century could attenuate the negative consequences of the permafrost carbon–climate feedback.

climate system | permafrost dynamics | carbon dynamics | permafrost carbon–climate feedback | soil carbon

A recent data-based synthesis has estimated that the release of soil carbon (C) to the atmosphere by 2100 from the northern permafrost region will be between 12 and 113 Pg C (10¹⁵ g) C for climate change pathways involving both substantive and little or no mitigation effort (1). This synthesis did not consider any response of vegetation production to climate change, which could offset this soil C release. In addition to the data synthesis approach, several process-based models have coupled thaw depth dynamics to the vertical distribution of soil C storage in the northern permafrost region (2). These models have the ability in principle to assess the potential vulnerability of

terrestrial C stocks to permafrost thaw in the context of vegetation production responses to climate change and CO₂ fertilization. A compilation of the responses of these models to climate pathways involving little or no mitigation (e.g., representative concentration pathway RCP8.5) has estimated losses of C from the permafrost region of between 37 and 174 Pg C by 2100 (mean, 92 Pg C) (3–5). One difficulty in comparing the results of these models is that they were driven by climate change output from different climate models. Furthermore, since these estimates

Significance

We applied regional and global-scale biogeochemical models that coupled thaw depth with soil carbon exposure to evaluate the dependence of the evolution of future carbon storage in the northern permafrost region on the trajectory of climate change. Our analysis indicates that the northern permafrost region could act as a net sink for carbon under more aggressive climate change mitigation pathways. Under less aggressive pathways, the region would likely act as a source of soil carbon to the atmosphere, but substantial net losses would not occur until after 2100. These results suggest that effective mitigation efforts during the remainder of this century could attenuate the negative consequences of the permafrost carbon–climate feedback.

Author contributions: A.D.M., D.M.L., and C.K. designed research; A.D.M., D.M.L., C.K., J.S.C., E.B., G.C., E.J., A.H.M., S.M., D.N., S.P., A.R., P.C., I.G., D.J.H., D.J., G.K., J.C.M., V.R., K.S., and Q.Z. performed research; A.D.M. and J.S.C. analyzed data; and A.D.M., D.M.L., C.K., J.S.C., E.B., G.C., E.J., A.H.M., S.M., D.N., S.P., A.R., P.C., I.G., D.J.H., D.J., G.K., J.C.M., V.R., C.S., K.S., E.A.G.S., and Q.Z. wrote the paper.

The authors declare no conflict of interest.

This article is a PNAS Direct Submission.

This open access article is distributed under [Creative Commons Attribution-NonCommercial-NoDerivatives License 4.0 \(CC BY-NC-ND\)](https://creativecommons.org/licenses/by-nc-nd/4.0/).

Data deposition: The simulation data analyzed in this manuscript are available through the National Snow and Ice Data Center (doi: [10.5067/ZRL5WJKN01XJM](https://doi.org/10.5067/ZRL5WJKN01XJM)).

¹To whom correspondence should be addressed. Email: admguire@alaska.edu.

This article contains supporting information online at www.pnas.org/lookup/suppl/doi:10.1073/pnas.1719903115/-DCSupplemental.

Published online March 26, 2018.

assumed little or no climate mitigation effort, it remains unclear to what extent climate mitigation policies may be effective in preventing the negative consequences of C release from the northern permafrost region. Finally, because C dynamics of the northern permafrost region may be nonlinear with time (6), it is important to assess how climate change may influence C dynamics after 2100 to inform decision makers on the long-term effectiveness of mitigation efforts.

To address these issues, the Permafrost Carbon Network (www.permafrostcarbon.org/) organized a multimodel assessment with “state-of-the-art” biogeochemical land models that coupled thaw depth with soil C exposure to evaluate (i) the contribution of model structural uncertainty and (ii) the potential impact of mitigation on the evolution of C storage in the northern permafrost region (Fig. 1) out to the year 2299. All models were forced with common climate projections (1, 7) for climate change pathways representative of substantive (RCP4.5 stabilization pathway) and little to no (RCP8.5 nonstabilization pathway) mitigation effort (see Fig. S1 for global and northern high-latitude temperature projections in comparison with other CMIP5 models); RCP4.5 and RCP8.5 are pathways that would result in preindustrial to 2100 radiative forcing being 4.5 W·m⁻² (~650 CO₂ equivalent) and 8.5 W·m⁻² (~1,370 CO₂ equivalent), respectively (8). To achieve the RCP4.5 pathway would require carbon emissions per energy consumption by global human society to decrease by 75% during this century (8). Our key questions in this analysis are as follows: (i) What is the variability in the projected loss of near-surface permafrost across models when forced with a common climate change trajectory (evaluated with eight models; Table 1)? (ii) What is the variability in projected changes of C stored in the permafrost region (soil and vegetation) for different representative mitigation pathways among model simulations (evaluated with five models; Table 1)? (iii) What factors explain the variability in the projected dynamics of C among the models (evaluated with three models; Table 1)? (iv) What are the implications for climate mitigation policies?

Results

Across the northern permafrost region, the 2010 estimates of the permafrost area (defined in our study as the area for which the simulated maximum seasonal active layer thickness is less than 3-m deep) ranged from 13.1 to 19.3 (mean, 14.1 ± 3.5 SD) × 10⁶ km² among the models. This range straddles the estimate of 16.2 × 10⁶ km² occupied by the continuous and discontinuous permafrost in the Northern Hemisphere (9). The 2010 estimates of soil C stock in the northern permafrost region ranged from 847 to 1,313 Pg C (mean, 1,104 ± 197 SD), which are comparable to an observationally based estimate of integrated C to 3 m in the northern permafrost region (1,035 ± 150 Pg C) (10). The 2010 estimates of vegetation C stocks among the models ranged from 39 to 218 Pg C (mean, 126 ± 64 SD), which bracket, but generally

overestimate, an observationally based estimate of vegetation C in tundra and boreal biomes (55 Pg C) (11, 12).

There were substantial differences in the projected loss of permafrost from 2010 through 2299 among model simulations [RCP4.5, Fig. 2A, mean loss of 4.1 (±0.6 SD) × 10⁶ km²; range loss of 3.2–4.6 × 10⁶ km²; RCP8.5, Fig. 2B, mean loss of 12.7 (±5.1 SD) × 10⁶ km²; range loss of 5.7–16.1 × 10⁶ km²] (Fig. 2A and B). The models generally agreed on the areal extent of near-surface permafrost loss except one simulation for the RCP8.5 climate trajectory, which projected only about one-half of the loss by 2299 relative to the other models. Among the models that ran sensitivity simulations, ~90% of the estimated permafrost loss was explained by model sensitivities to changes in air temperature (warming effect in Fig. 2C and D).

Between 2010 and 2299, the model simulations of soil C for the RCP4.5 projection varied from gains of 70 Pg C to losses of 67 Pg C (mean 3-Pg C gain ± 50-Pg C SD; Fig. 3A). For the RCP8.5 projection, all of the models projected large net losses of soil C by 2299 that ranged from 74 to 652 Pg C (mean 341-Pg C loss ± 242-Pg C SD; Fig. 3B). Although all of the models projected net losses of soil C by 2299 for the RCP8.5 projection, the trajectories of soil C dynamics differed substantially among the models, with some models indicating that net soil C losses will occur throughout the projection period and others indicating that there would be a period of net soil C gain before losses ensued. The models also differed in the relative amount of soil C that would be lost by 2299 with three models losing less than 20% vs. two models that lost 50% and 63% of their initial soil C stock in 2010. Among the three models that ran sensitivity simulations, temperature changes were ~16 times more important than precipitation changes in causing losses of net soil C for the RCP8.5 scenario.

Between 2010 and 2299, four of the five models indicated gains in vegetation C of up to 175 (mean, 69 ± 70 SD) Pg C for the RCP4.5 projection (Fig. 3C; one model estimated a loss of 3 Pg C) and all of the models indicated gains (10- to 363-Pg C gains; mean, 132 ± 148 SD Pg C) for the RCP8.5 projection (Fig. 3D). In the simulations for the RCP4.5 projection, the gains in vegetation C were largely responsible for the overall projected net gains in ecosystem C by 2299 (8- to 244-Pg C gains; mean, 71 ± 99 SD Pg C; Fig. 3E). In contrast, for the RCP8.5 projection, gains in vegetation C were not great enough to compensate for the losses of C projected by four of the five models, so that net changes in ecosystem C ranged from a loss of 641 Pg C to a gain of 167 Pg C by 2299 (mean loss, 208 Pg C ± 307 SD Pg C; Fig. 3F). Although the models disagreed as to whether net losses of ecosystem C would begin before or after 2100, all of the models indicated that substantial net losses of ecosystem C would not occur until after 2100 as a result of vegetation gain offsetting any soil C losses (Fig. 3F).

To gain a greater understanding of the variation in model responses, we analyzed the sensitivity of net primary production (NPP) and heterotrophic respiration (HR) to changes in atmospheric CO₂ (given no change in climate), mean annual air temperature (given no other changes in climate and CO₂), and annual precipitation (given no other changes in climate and CO₂) at the regional scale for three of the models. This analysis indicates that both NPP and HR were quite sensitive to changes in atmospheric CO₂ (Fig. 4A and B; see Fig. S2A and B for CO₂ sensitivity of HR). For the RCP4.5 projection, the sensitivity analysis indicates that NPP increases between 0.09 and 0.58 gC·m⁻²·y⁻¹·ppmv⁻¹ CO₂ (Fig. 4A), which is between 1.9% and 15.4% increase per 100 ppmv CO₂, among the models. For the RCP8.5 projection, NPP has a similar range in sensitivity to atmospheric CO₂ until the increase in atmospheric CO₂ is more than ~500 ppmv greater than the 2010 level (Fig. 4B, a point reached at 2095), at which point the response starts to saturate. For the model with N limitation of photosynthetic assimilation (TEM6), NPP saturation is essentially complete for a CO₂ increase of 800 ppmv, but NPP of the other models is not yet saturated for a CO₂ increase of 1,600 ppmv.

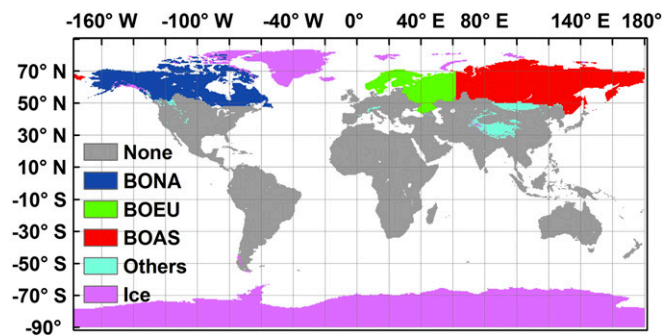


Fig. 1. The spatial extent of the permafrost region in the Northern Hemisphere defined in this study. Subregions include boreal Asia (BOAS), boreal Europe (BOEU), boreal North America (BONA), Glaciers and Ice Sheets (Ice), and other permafrost areas (Other). Reprinted with permission from ref. 2.

Table 1. Models used in this study to assess responses of permafrost dynamics, carbon dynamics, and sensitivity of carbon dynamics to changes in atmospheric CO₂, air temperature, and precipitation

Model acronym	Model name	Used to simulate		Used to evaluate
		permafrost dynamics	carbon dynamics	sensitivity of carbon dynamics
CLM4.5	Community Land Model, Version 4.5	Yes	Yes	No
CoLM	Common Land Model	Yes	No	No
JULES	Joint UK Land Environmental Simulator	Yes	No	No
ORCHb	Orchidee Land Model, Version b*	Yes	Yes	Yes
UVic	University of Victoria Earth System Climate Model	Yes	Yes	Yes
TEM6	Terrestrial Ecosystem Model, Version 6	Yes	Yes	Yes
SIBCASA	Simple Biosphere/Carnegie-Ames-Stanford Approach Model	Yes	Yes	No
GIPLb	Geophysical Institute Permafrost Lab Model, Version b [†]	Yes	No	No

*ORCHb considers depth of carbon dynamics to 47 m in the soil column, in comparison with 2 m in ORCHa.

[†]GIPLb increases snow density as it accumulates on the ground surface, in comparison with empirical snow warming factors in GIPL.

The analyses of air temperature sensitivities (i.e., warming effect in Fig. 4) for the RCP4.5 projection indicate that HR, the sensitivity of which includes both per-gram sensitivity combined with the quantity of soil C exposed to decomposition, is more sensitive to changes in air temperature ($6.44\text{--}22.10\text{ gC}\cdot\text{m}^{-2}\cdot\text{y}^{-1}\cdot\text{C}^{-1}$; Fig. 4E) than NPP ($4.48\text{--}21.90\text{ gC}\cdot\text{m}^{-2}\cdot\text{y}^{-1}\cdot\text{C}^{-1}$; Fig. 4C) for each of the models. The air temperature sensitivity of HR for the RCP8.5 projection ($12.64\text{--}59.99\text{ gC}\cdot\text{m}^{-2}\cdot\text{y}^{-1}\cdot\text{C}^{-1}$ through $+8.62\text{ }^{\circ}\text{C}$; Fig. 4F) is greater than that for the RCP4.5 projection, although the sensitivity tends to decline above approximately $+8.5\text{ }^{\circ}\text{C}$. For the RCP8.5 projection, HR (Fig. 4F) is quite a bit more sensitive than NPP (Fig. 4D) for the UVic model (59.99 vs. $31.82\text{ gC}\cdot\text{m}^{-2}\cdot\text{y}^{-1}\cdot\text{C}^{-1}$), slightly more sensitive for the ORCHb model (12.64 vs. $11.07\text{ gC}\cdot\text{m}^{-2}\cdot\text{y}^{-1}\cdot\text{C}^{-1}$), but less sensitive for the TEM6 model (16.43 vs. $25.26\text{ gC}\cdot\text{m}^{-2}\cdot\text{y}^{-1}\cdot\text{C}^{-1}$) until approximately $+5\text{ }^{\circ}\text{C}$. After approximately $+5\text{ }^{\circ}\text{C}$, the TEM6 NPP sensitivity becomes negative ($-13.25\text{ gC}\cdot\text{m}^{-2}\cdot\text{y}^{-1}\cdot\text{C}^{-1}$). Our analyses indicated that there was little sensitivity to changes in precipitation for model responses of NPP (Fig. S2 C and D) and HR (Fig. S2 E and F).

Discussion and Conclusions

It is important to assess the degree to which the climate system is sensitive to the loss of C in the permafrost region. However, most land models that are being used within earth system

models, which are being developed to consider how interactions among physical, biological, and human systems influence climate, do not yet represent the linkage between permafrost and soil C dynamics needed to confidently assess the response of C in the northern permafrost region to projected climate change. Syntheses of models that do represent this linkage estimate that the feedback to the climate system from the decomposition of frozen soil C in permafrost could add up to $0.27\text{ }^{\circ}\text{C}$ additional global warming by 2100 and up to $0.42\text{ }^{\circ}\text{C}$ by 2300 for climate change scenarios that represent little or no mitigation effort (4, 5, 13).

The vulnerability of permafrost and ecosystem C pools in the permafrost region depends in part on the exposure of permafrost C to changes in atmospheric CO₂ and climate. This study analyzed this vulnerability for climate change projections that represented both substantive and little/no mitigation effort. Our analysis indicates that the northern permafrost region could act as a net sink for C (that includes both changes in both vegetation and soil C) under more aggressive climate change mitigation pathways, which both process-based and atmospheric inversion models suggest has been happening in recent decades (2, 14). Although enhanced NPP could maintain the net sink under aggressive mitigation pathways, it is important to realize that, during this century and beyond, soil C in permafrost will be exposed to decomposition once thawed under any warming pathway, a portion of which will be lost to the atmosphere. Under less aggressive mitigation pathways, the region would likely act as a net source of C to the atmosphere, as noted by previous syntheses (1, 3), but substantial net losses of C would not occur until after 2100. These results suggest that effective mitigation efforts during the remainder of this century could substantially attenuate the negative consequences of net C releases from the permafrost region.

This conclusion is tempered by three primary sources of uncertainty, one of which is associated with climate forcing, one of which is associated with model structural and functional deficiencies, and one of which is associated with variability in the sensitivity of the models to climate forcing. We only used the climate projections from one earth system model in the CMIP5 archive to facilitate comparison of sensitivity to forcing among the models. We considered the CCSM4 CMIP5 climate projections both appropriate and representative projections from the CMIP5 archive because of (i) the substantial effort that has gone into representing permafrost in CCSM4 (15–17), (ii) the rate of warming projected by CCSM4 is an intermediate rate in the northern permafrost region compared with the other earth system models in the CMIP5 archive (Fig. S1) (18), and (iii) CCSM4 was among the higher performing models with respect to present-day temperature and precipitation trajectories over the northern permafrost region (8).

It is important to recognize that biogeochemical models generally applied in the northern permafrost region have known structural and functional deficiencies (19), such as the representation of moss dynamics. Although the models in this study

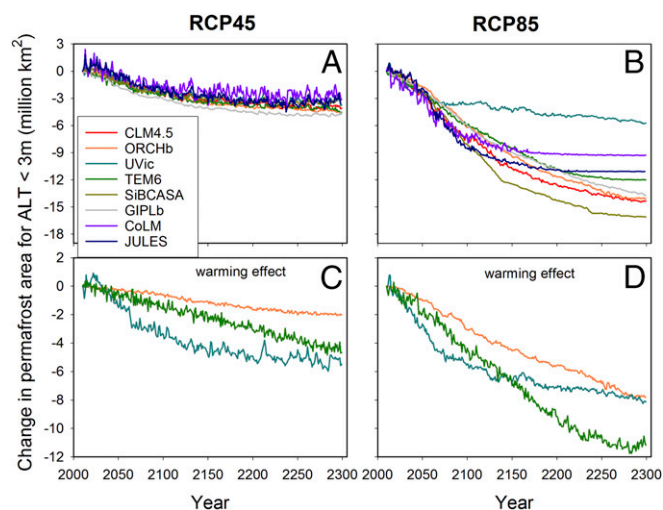


Fig. 2. Changes in simulated permafrost dynamics. Simulated cumulative changes in (A and B) permafrost area for active layer thickness (ALT) less than 3 m from 2010 to 2299 and (C and D) the sensitivity of simulated changes in permafrost area to changes in mean annual air temperature for the CCSM4 model (Left column) RCP4.5 and (Right column) RCP8.5 projections.

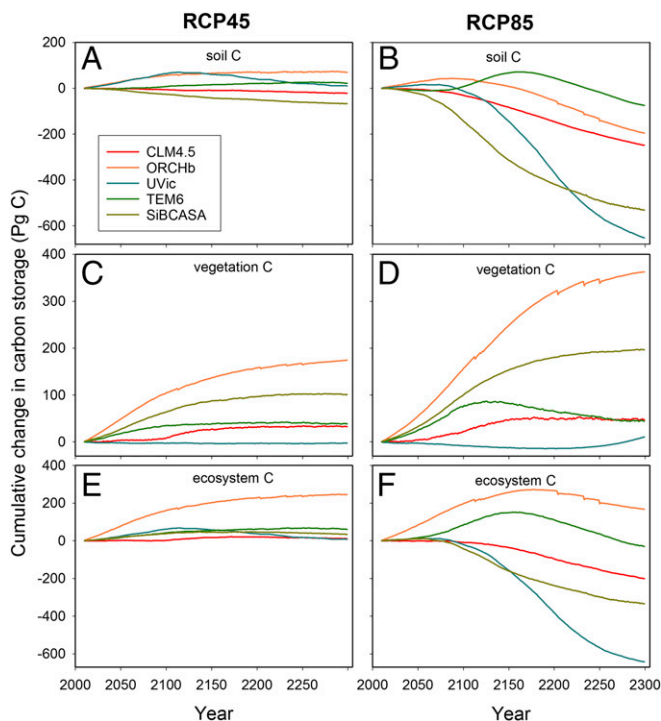


Fig. 3. Changes in simulated carbon storage. Simulated cumulative changes in (A and B) soil, (C and D) vegetation, and (E and F) total ecosystem carbon storage between 2010 and 2299 for the CCSM4 model (Left column) RCP4.5 and (Right column) RCP8.5 projections.

implicitly consider moss to be part of vegetation biomass, moss is static in the permafrost component of these models (Table S1) and the models do not explicitly couple moss C dynamics to soil C dynamics (Table S2). Moss can be an important component of the vegetation in some ecosystems of the northern permafrost region. For example, moss comprises 40% of biomass in sedge tundra ecosystems (20). Even though the models in this study have some deficiencies with respect to modeling the full dimensions of C dynamics in the northern permafrost region, it is important to recognize that earth system models in general do not include any representation of the permafrost carbon–climate feedback because the land models generally used in earth system models have not yet included vertically resolved C dynamics in the soil. Thus, this study provides an important comparison point for future efforts to evaluate the permafrost carbon–climate feedback by the earth system model community as they become more capable of evaluating the magnitude of the permafrost carbon–climate feedback.

A step toward reducing uncertainty in the range of additional warming estimated by fully coupled earth system models is to better understand the sources of uncertainty among the carbon models used in earth system models (21). The performance and sensitivity of the permafrost and biogeochemistry models used in this study to historical changes in atmospheric CO₂ and climate have been evaluated in the northern permafrost region in several previous studies conducted by the Permafrost Carbon Network (2, 22–25). These analyses have provided the basis for improving models through constraining model sensitivities based on experimental- and field-based syntheses (26–28).

The sensitivities of model NPP responses to changes in atmospheric CO₂ for RCP4.5 were between 1.9% and 15.4% increase in NPP per 100-ppmv CO₂ before saturation, which is generally consistent with syntheses of free-air exchange CO₂ enrichment (FACE) experiments (mean of 13% globally) (29). However, it is important to recognize that these syntheses primarily represent FACE experiments that were conducted in

temperate forests. Thus, there is the need for FACE experiments in the northern permafrost region to better constrain model responses to enhance atmospheric CO₂ in the region. In this study, the model with the least sensitivity (TEM6) was the only model in the sensitivity analysis for which C uptake was limited by plant N dynamics. Because the CO₂ response of the northern permafrost region is expected to be damped by N limitation (30, 31), it is important for earth system models to make progress in implementing N limitation to more effectively constrain analyses of the permafrost carbon–climate feedback.

Although the response to CO₂ fertilization is the primary reason for increases in C storage simulated by the models, models did exhibit substantial sensitivity of NPP to changes in air temperature. In recent decades, increasing temperatures appear to have increased plant biomass in tundra (32, 33), although some recent studies indicate that the long-term trend of greening in tundra may be experiencing a reversal in this decade (34, 35). Some analyses suggest that productivity in boreal forest regions has decreased in recent decades (36). In contrast, models generally indicate that NPP and vegetation C in the northern permafrost region have increased historically (2) and will continue to increase in the future (this study). It is important to recognize that there are some potentially important interactions of the NPP response to both changes in atmospheric CO₂ and temperature. For example, models that include N dynamics can predict increases in NPP in response to warming because of increased nitrogen availability released as a consequence of increased HR in response to warming (37), which may work against the N limitation of NPP to enhanced atmospheric CO₂. This response of NPP to enhanced N availability from soil warming occurs in TEM6, and is largely the reason why the

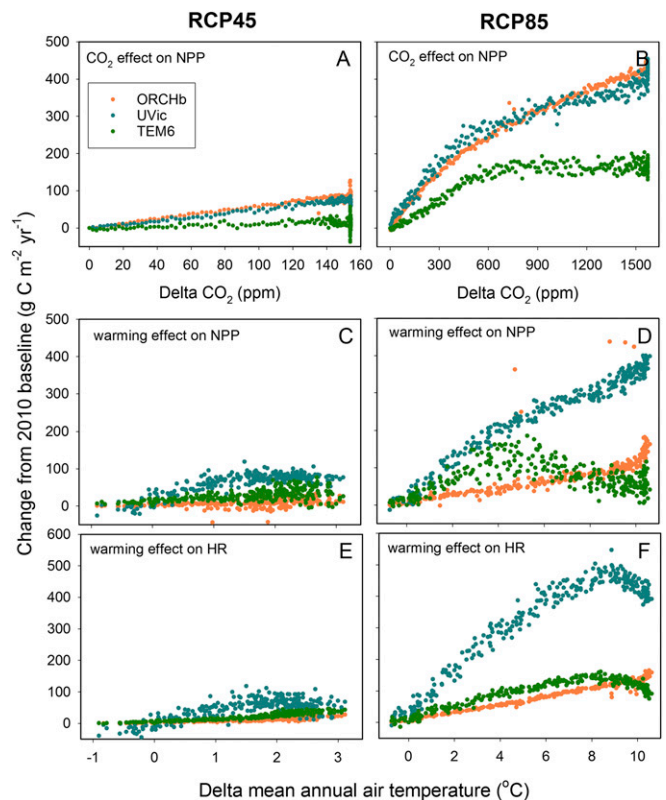


Fig. 4. The sensitivity of carbon dynamics to changes in atmospheric CO₂ and temperature. The sensitivity of simulated (A and B) net primary production (NPP) to changes in atmospheric CO₂, (C and D) NPP to changes in mean annual air temperature, and (E and F) heterotrophic respiration (HR) to changes in mean annual air temperature for the CCSM4 model (Left column) RCP4.5 and (Right column) RCP8.5 projections.

model does not have as large a loss of soil C that would be expected because of N limitation to enhanced atmospheric CO₂. In addition, warming may lengthen the growing season to allow vegetation to take up more CO₂ from the atmosphere. Because the responses of ecosystem C among the models in this study depend substantially on the responses of NPP, which has a complicated response to changes in CO₂ and temperature, it is important to better reconcile the NPP sensitivity of the models to changes in atmospheric CO₂ and temperature with observation-based analyses of changes in productivity and biomass.

In general, the models indicate that HR is more sensitive to temperature change than NPP, and that HR is much more sensitive in the RCP8.5 simulations than the RCP4.5 simulations as more soil C becomes exposed to decomposition because of deeper permafrost thaw. This variability in temperature sensitivity, combined with variability in CO₂ sensitivity, leads to substantial uncertainty in the timing and magnitude of the permafrost carbon–climate feedback. Data to constrain the HR responses to warming have recently been synthesized (27). In addition, a recently introduced metric for soil C residence time may also help constrain the models (38).

Despite model uncertainties, the results of this study indicate that, under climate change trajectories resulting from little or no mitigation effort, such as the RCP8.5 climate we considered, the northern permafrost region would likely act as a source of soil carbon to the atmosphere, but substantial net losses would not occur until after 2100. Under climate change trajectories resulting from more aggressive mitigation, such as the RCP4.5 climate we considered, our analysis indicates that the northern permafrost region could act as a net sink for carbon. These results have significant implications for climate mitigation policies, as they indicate that effective mitigation policies could attenuate the negative consequences of the permafrost–carbon feedback that are likely to occur under policies that result in little or no mitigation.

Methods

The spatial domain of the permafrost region in the Northern Hemisphere that we considered in this study (Fig. 1; 30.88 × 10⁶ km²) was defined based on (i) the location of glaciers and ice sheets in the Northern Hemisphere, (ii) the extent of the boreal Asia, boreal Europe, and boreal North America regions (39), and (iii) other permafrost areas outside of these areas identified as part of the northern permafrost domain in a permafrost and ground ice condition map (40). The models in this study did not simulate permafrost and C dynamics for glacier and ice sheet area. The areas of boreal Asia, Europe, and North America facilitate comparisons with inversion model analyses of the C cycle. The “Other” area includes areas of Tibet and various mountain ranges in the Northern Hemisphere as well as areas just south of boreal Asia that are considered part of the permafrost region (40).

All models were driven with a common projection period forcing by applying monthly climate anomalies/scale factors from a CCSM4 simulation that included the RCP4.5 and RCP8.5 (2006–2100) (41) and the extended concentration pathways (ECP4.5 and ECP8.5, 2101–2299) (42) on top of repeating early 20th century reanalysis forcing. The historical (before 2010) driving datasets in this study were model dependent as a number of models were involved in activities that relied on the use of different retrospective forcing datasets. Therefore, each modeling group was free to choose appropriate driving datasets for climate, atmospheric CO₂, N deposition, disturbance, soil texture, and other forcing data. The historical driving datasets used by each model were documented in table 3 of McGuire et al. (2). The spin-up process was also specific to each model, but it was conducted to support the delivery of simulation results starting in 1960. Guidance was provided from the Permafrost Carbon Network modeling group on how to apply the monthly anomalies, but each modeling group was responsible for harmonizing the historical and future datasets that were to be used for driving their models. The same time series for global atmospheric carbon dioxide concentrations was used to drive all models.

Compared with other earth system models, the CCSM4 simulations we used for forcing projected intermediate levels of temperature change for both global and northern high latitudes domains for both RCP4.5/ECP4.5 and RCP8.5/ECP8.5 pathways (Fig. S1). CCSM4 was among the higher performing models with respect to the mean present-day temperature bias across the northern permafrost region (8). In general, the temperature and precipitation trajectories over the northern permafrost region projected by

CCSM4 for RCP4.5 and RCP8.5 did not diverge until around 2040. However, divergence was substantial after 2040, with these variables for RCP4.5 more or less stable by 2100, while for RCP8.5 these variables were not stable even by 2299. Between the decades of 2010–2019 and 2290–2299, the CCSM4 simulations for the RCP4.5 and RCP8.5 pathways, respectively, project that over the northern permafrost region (i) mean annual air temperature will increase by 2.6 and 12.8 °C; (ii) annual precipitation will increase 37 and 137 mm; (iii) down-welling surface short wave radiation will decrease 1.5 and 4.8 W·m⁻²; (iv) down welling surface long-wave radiation will increase 12.3 and 64.1 W·m⁻², and (v) near-surface specific humidity will increase 0.00047 and 0.00280 kg·kg⁻¹.

Our analysis of simulated permafrost dynamics focuses on changes in near-surface permafrost area between 2010 and 2299. While there are many different ways to define and estimate the presence of near-surface permafrost [Wang et al. (23)], we operationally define the area of near-surface permafrost in this study as the area simulated in which the maximum seasonal active layer thickness (ALT) is less than 3 m, that is, where the bulk of the frozen C is located (43).

Our analysis of the variability in the sensitivity of C focuses on changes in soil C, vegetation C, and total ecosystem C between 2010 and 2299. Soil C is an aggregated variable that is the sum of estimates for litter C, organic horizon C, mineral soil C, coarse woody debris, land use pools (e.g., wood and agricultural products), and soil C exudates reported by some models. Vegetation C is the sum of any live vegetation pool and typically includes leaves, stems, and root C. Although the models in this study did not consider moss to be an explicit dynamic compartment in the vegetation, they either lumped moss biomass/NPP into a leaf compartment or into the aggregated vegetation biomass/NPP so that it is considered implicitly as part of the vegetation C dynamics. Ecosystem C is the sum of the aggregated soil and vegetation C pools.

The fluxes we considered in this study for calculating C balance included NPP, HR, fire emissions (Fire C), biogenic CH₄ emissions (BIO C-CH₄), and lateral C fluxes. NPP is the net uptake of CO₂ by vegetation and represents the difference between photosynthetic uptake and plant respiration. HR is the release of CO₂ to the atmosphere associated with decomposition of dead organic matter. Fire C is the release of C-related compounds to the atmosphere from the combustion of above- and below-ground C pools during fire. We assumed that all of Fire C is CO₂ since the models did not distinguish among species of C emitted (i.e., CO₂, CO, and pyrogenic CH₄). BIO C-CH₄ represents biogenic CH₄ emissions to the atmosphere from the production of methane by methanogenic organisms in the soil minus any uptake in the soil column by methanotrophic organisms. In general, the models in this study do not explicitly consider the CH₄ emissions from lakes in the permafrost region, although their definition of the spatial extent of wetlands may include lakes. Lateral C includes any lateral losses of C from the ecosystem C pools that we do not directly estimate in the balance with the atmosphere, and include the lateral transfer of harvest products from agriculture, forestry, and land use, as well as C fluxes to aquatic ecosystems such as dissolved organic C. Note that some proportion of lateral C is returned to that atmosphere at the regional scale, but the models in this study do not estimate that proportion.

In this study, we compare permafrost and C dynamics of the permafrost region between 2010 and 2299 among five models that have focused on representing soil C explicitly with depth in permafrost regions. Our comparison of permafrost dynamics also included three other models that did not model C explicitly with depth. The model simulations of both permafrost and C dynamics analyzed in this study include those from (i) the Community Land Model (CLM4.5, version 4.5) (44, 45), (ii) the ORCHIDEE-IPSL model (ORCHb) (46–49), (iii) the SiBCASA land model (SiBCASA) (50), (iv) version 6 of the Terrestrial Ecosystem Model (TEM6) (39, 51), and (v) the University of Victoria Earth System Climate Model (UVic) (6, 52). Our analysis of permafrost dynamics also used the Geophysical Institute Permafrost Lab model (GIPLb) (53), the Common Land Model (CoLM) (54, 55), and the Joint UK Land Environment Simulator (JULES) (56, 57). The key features that influence soil thermal dynamics of these models are compared in Table S1. The key structural features that influence permafrost region C dynamics of the models are compared in Table S2.

To determine the relative effects of the atmospheric temperature, CO₂, and precipitation drivers on the C cycle responses of the models, we conducted three additional simulations in addition to the simulation with all of the drivers. A subset of the models performed separate simulations with (i) detrended air temperature, (ii) constant CO₂, and (iii) detrended temperature and precipitation [see table 4 of McGuire et al. (2)]. Three of the five models that were analyzed for C dynamics in this study provided results from these ancillary simulations (ORCHb, TEM6, and UVic). The effects of changes in temperature (Fig. 2 for changes in permafrost area, Fig. 4) and

atmospheric CO₂ (Fig. 4 and Fig. S2) between 2010 and 2299 were estimated by subtracting the results of the detrended air temperature and constant CO₂ simulations, respectively, from the simulation with all drivers. The effect of changes in precipitation (Fig. S2) was estimated by subtracting the detrended temperature and precipitation simulation from the detrended air temperature simulation.

ACKNOWLEDGMENTS. Support for this study was provided by the National Science Foundation through the Research Coordination Network program and through the Study of Environmental Arctic Change program in support of the Permafrost Carbon Network. Support was also provided by the

National Science Foundation and the US Department of Agriculture Forest Service in support of the Bonanza Creek Long-Term Ecological Research, the US Department of Energy Office of Science (Biological and Environmental Research), the University of Victoria, Natural Sciences and Engineering Research Council (NSERC) Canada Graduate Scholarships, NSERC Collaborative Research and Training Experience, Joint Department of Energy and Climate Change/Defra Met Office Hadley Centre Climate Programme (GA01101), and the European Commission Seventh Framework Programme project PAGE21 (Grant 282700). Any use of trade, firm, or product names is for descriptive purposes only and does not imply endorsement by the US Government.

- Koven CD, et al. (2015) A simplified, data-constrained approach to estimate the permafrost carbon-climate feedback. *Philos Trans R Soc A* 373:20140423.
- McGuire AD, et al. (2016) Variability in the sensitivity among model simulations of permafrost and carbon dynamics in the permafrost region between 1960 and 2009. *Global Biogeochem Cycles* 30:1015–1037.
- Schuur EAG, et al. (2015) Climate change and the permafrost carbon feedback. *Nature* 520:171–179.
- Schaefer K, Lantuit H, Romanovsky VE, Schuur EAG (2012) *Policy Implications of Thawing Permafrost*, United Nations Environment Programme Special Report (United Nations Environment Programme, Nairobi, Kenya), DEW/1621/NA.
- Schaefer K, Lantuit H, Romanovsky VE, Schuur EAG, Witt R (2014) The impact of the permafrost carbon feedback on global climate. *Environ Res Lett* 9:085003.
- MacDougall AH, Avis CA, Weaver AJ (2012) Significant existing commitment to warming from the permafrost carbon feedback. *Nat Geosci* 5:719–721.
- Lawrence DM, Koven CD, Swenson SC, Riley WJ, Slater AG (2015) Permafrost thaw and resulting soil moisture changes regulate projected high-latitude CO₂ and CH₄ emission. *Environ Res Lett* 10:094011.
- van Vuuren DP, et al. (2011) The representative concentration pathways: An overview. *Clim Change* 109:5–31.
- Slater AG, Lawrence DM (2013) Diagnosing present and future permafrost from climate models. *J Clim* 26:5608–5623.
- Hugelius G, et al. (2014) Estimated stocks of circumpolar permafrost carbon with quantified uncertainty ranges and identified data gaps. *Biogeosciences* 11:6573–6593.
- Neigh CSR, et al. (2013) Taking stock of circumboreal forest carbon with ground measurements, airborne and spaceborne LiDAR. *Remote Sens Environ* 137:274–287.
- Raynolds MK, Walker DA, Epstein HE, Pinzon JE, Tucker CJ (2012) A new estimate of tundra-biome phytomass from trans-Arctic field data and AVHRR NDVI. *Remote Sens Lett* 3:403–411.
- Burke EJ, et al. (2017) Quantifying uncertainties of permafrost carbon-climate feedbacks. *Biogeosciences* 14:3051–3066.
- McGuire AD, et al. (2009) Sensitivity of the carbon cycle in the Arctic to climate change. *Ecol Monogr* 79:523–555.
- Lawrence DM, Slater AG, Romanovsky VE, Nicolsky DJ (2008) The sensitivity of a model projection of near-surface permafrost degradation to soil column depth and inclusion of soil organic matter. *J Geophys Res* 113:F02011.
- Lawrence DM, Slater AG, Swenson S (2012) Simulation of present-day and future permafrost and seasonally frozen ground conditions in CCSM4. *J Clim* 25:2207–2225.
- Lawrence DM, Slater AG (2010) The contribution of snow condition trends to future ground climate. *Clim Dyn* 34:969–981.
- Koven CD, Riley WJ, Stern A (2013) Analysis of permafrost thermal dynamics and response to climate change in the CMIP5 earth system models. *J Clim* 26:1877–1900.
- Fisher JB, et al. (2018) Missing pieces to modeling the Arctic-Boreal puzzle. *Environ Res Lett*, in press.
- Euskirchen ES, McGuire AD, Chapin FS, 3rd, Yi S, Thompson CC (2009) Changes in vegetation in northern Alaska under scenarios of climate change, 2003–2100: Implications for climate feedbacks. *Ecol Appl* 19:1022–1043.
- Luo Y, et al. (2016) Toward more realistic projections of soil carbon dynamics by earth system models. *Global Biogeochem Cycles* 30:40–56.
- Xia J, et al. (2017) Terrestrial ecosystem model performance in simulating productivity and its vulnerability to climate change in the northern permafrost region. *J Geophys Res Biogeosci* 122:430–446.
- Wang W, et al. (2016) Evaluation of air-soil temperature relationships simulated by land surface models during winter across the permafrost region. *Cryosphere* 10:1721–1737.
- Peng S, et al. (2016) Simulated high-latitude soil thermal dynamics during the past 4 decades. *Cryosphere* 10:179–192.
- Rawlins M, et al. (2015) Assessment of model estimates of land-atmosphere CO₂ exchange across northern Eurasia. *Biogeosciences* 12:4385–4405.
- Olefeldt D, Turetsky MR, Crill PM, McGuire AD (2013) Environmental and physical controls on northern high latitude methane fluxes across permafrost zones. *Glob Chang Biol* 19:589–603.
- Schädel C, et al. (2016) Potential carbon emissions dominated by carbon dioxide from thawed permafrost soils. *Nat Clim Chang* 6:950–953.
- Treat CC, et al. (2015) A pan-Arctic synthesis of CH₄ and CO₂ production from anoxic soil incubations. *Glob Chang Biol* 21:2787–2803.
- Piao S, et al. (2013) Evaluation of terrestrial carbon cycle models for their response to climate variability and to CO₂ trends. *Glob Chang Biol* 19:2117–2132.
- McGuire AD, Melillo JM, Joyce LA (1995) The role of nitrogen in the response of forest net primary production to elevated atmospheric carbon dioxide. *Annu Rev Ecol Syst* 26:473–503.
- McGuire AD, et al. (1997) Equilibrium responses of global net primary production and carbon storage to doubled atmospheric carbon dioxide: Sensitivity to changes in vegetation nitrogen concentration. *Global Biogeochem Cycles* 11:173–189.
- Frost GV, Epstein HE (2014) Tall shrub and tree expansion in Siberian tundra ecotones since the 1960s. *Glob Chang Biol* 20:1264–1277.
- Ju J, Masek JG (2016) The vegetation greenness trend in Canada and US Alaska from 1984–2012 Landsat data. *Remote Sens Environ* 176:1–16.
- Epstein HE, et al. (2015) Tundra greenness. *Arctic Report Card: Update for 2015*, eds Jeffries MO, Richter-Menge J, Overland JE. Available at www.arctic.noaa.gov/Report-Card/Report-Card-2015/ArtMid/5037/ArticleID/221/Tundra-Greenness. Accessed January 15, 2018.
- Phoenix GK, Bjerke JW (2016) Arctic browning: Extreme events and trends reversing arctic greening. *Glob Chang Biol* 22:2960–2962.
- Beck PSA, Goetz SJ (2011) Satellite observations of high northern latitude vegetation productivity changes between 1982 and 2008: Ecological variability and regional differences. *Environ Res Lett* 6:049501.
- McGuire AD, et al. (1992) Interactions between carbon and nitrogen dynamics in estimating net primary productivity for potential vegetation in North America. *Global Biogeochem Cycles* 6:101–124.
- Koven CD, Hugelius G, Lawrence DM, Wieder WR (2017) Higher climatological temperature sensitivity of soil carbon in cold than warm climates. *Nat Clim Chang* 7: 817–822.
- Hayes DJ, et al. (2011) Is the northern high-latitude land-based CO₂ sink weakening? *Global Biogeochem Cycles* 25:GB3018.
- Brown J, Ferrans OJ, Jr, Heginbottom JA, Melnikov ES (1998) *Circum-Arctic Map of Permafrost and Ground-Ice Conditions* (National Snow and Ice Data Center/World Data Center for Glaciology, Boulder, CO), Digital Media, revised February 2001.
- Meehl GA, et al. (2013) Climate change projections in CESM1(CAM5) compared to CCSM4. *J Clim* 26:6287–6308.
- Randerson JT, et al. (2015) Multicentric changes in ocean and land contributions to the climate-carbon feedback. *Global Biogeochem Cycles* 29:744–759.
- Hugelius G (2012) Spatial upscaling using thematic maps: An analysis of uncertainties in permafrost soil carbon estimates. *Global Biogeochem Cycles* 26:GB2026.
- Oleson KW, et al. (2013) Technical Description of Version 4.5 of the Community Land Model (CLM) (National Center for Atmospheric Research, Boulder, CO), Technical Note NCAR/TN-503+STR.
- Koven CD, et al. (2013) The effect of vertically-resolved soil biogeochemistry and alternate soil C and N models on C dynamics of CLM4. *Biogeosciences* 10: 7109–7131.
- Koven CD, et al. (2009) On the formation of high-latitude soil carbon stocks: Effects of cryoturbation and insulation by organic matter in a land surface model. *Geophys Res Lett* 36:L21501.
- Koven CD, et al. (2011) Permafrost carbon-climate feedbacks accelerate global warming. *Proc Natl Acad Sci USA* 108:14769–14774.
- Gouttevin IM, et al. (2012) How the insulating properties of snow affect soil carbon distribution in the continental pan-Arctic area. *J Geophys Res Biogeosci* 117:G02020.
- Gouttevin IM, Krinner G, Ciais P, Polcher J, Legout C (2012) Multi-scale validation of a new soil freezing scheme for a land-surface model with physically-based hydrology. *Cryosphere* 6:407–430.
- Schaefer K, Zhang T, Bruhwiler L, Barrett AP (2011) Amount and timing of permafrost carbon release in response to climate warming. *Tellus* 63B:165–180.
- Hayes DJ, et al. (2014) The impacts of recent permafrost thaw on land-atmosphere greenhouse gas exchange. *Environ Res Lett* 9:045005.
- Avis CA, Weaver AJ, Meissner KJ (2011) Reduction in areal extent of high-latitude wetlands in response to permafrost thaw. *Nat Geosci* 4:444–448.
- Nicolsky DJ, Romanovsky VE, Panteleev GG (2009) Estimation of soil thermal properties using in-situ temperature measurements in the active layer and permafrost. *Cold Res Sci Technol* 55:120–129.
- Dai Y, et al. (2003) The common land model (CLM). *Bull Am Meteorol Soc* 84: 1013–1023.
- Ji D, et al. (2014) Description and basic evaluation of Beijing Normal University earth system model (BNU-ESM) version 1. *Geosci Model Dev* 7:2039–2064.
- Best MJ, et al. (2011) The joint UK land environment simulator (JULES), model description—Part 1: Energy and water fluxes. *Geosci Model Dev* 4:677–699.
- Clark DB, et al. (2011) The joint UK land environment simulator (JULES), model description—Part 2: Carbon fluxes and vegetation dynamics. *Geosci Model Dev* 4: 701–722.